

Self-interstitial aggregation in diamond

J. P. Goss, B. J. Coomer, and R. Jones

School of Physics, The University of Exeter, Exeter EX4 4QL, United Kingdom

T. D. Shaw, P. R. Briddon, and M. Rayson

Department of Physics, The University of Newcastle upon Tyne, Newcastle upon Tyne NE1 7RU, United Kingdom

S. Öberg

Department of Mathematics, Luleå University of Technology, Luleå SE-97187, Sweden

(Received 26 September 2000; revised manuscript received 10 January 2001; published 30 April 2001)

First-principles methods are used to investigate the self-interstitial and its aggregates in diamond. The experimental assignment of the spin-1 $R2$ EPR center to the single interstitial has been questioned because of the small fine-structure term observed. We calculate the spin-spin interaction tensor for the three interstitial defects $I_1^{(001)}$, I_2^{NN} , and I_3 and compare with the experimental D tensors. The results give support for the assignments of the single and di-interstitials to microscopic models and allow us to conclusively identify a recently observed EPR center, $O3$, with I_3 . This identification, in turn, suggests a low-energy structure for I_4 and a generic model for an extended defect called the platelet. We also determine the optical properties of $I_1^{(001)}$ as well as its piezospectroscopic or stress tensor and find these to be in agreement with experiment. Several multi-interstitial defects are found to possess different structural forms which may coexist. We propose that a different form of the charged I_2 defect gives rise to the $3H$ optical peak. Several structures of the platelet are considered, and we find that the lowest-energy model is consistent with microscopic and infrared studies.

DOI: 10.1103/PhysRevB.63.195208

PACS number(s): 61.72.Ji, 61.80.Az, 63.20.Pw, 71.55.Cn

I. INTRODUCTION

The thorough understanding of self-interstitials and the processes by which they aggregate has become an important goal throughout the semiconductor defect field. For example, the increasing use of silicon devices in high-radiation environments has prompted numerous investigations into the complex process of self-interstitial aggregation during annealing which leads to the generation of extended rod-like $\{113\}$ defects. The structure of these aggregates is now well characterized,¹ yet the structures of small interstitial aggregates and the self-interstitial itself are still under debate.²⁻⁴

In diamond the current state of knowledge is quite different. Although the extended interstitial defect known as the platelet has received much attention from experimentalists,⁵⁻⁹ the structure, and even the composition, of the defect is still the subject of debate. On the other hand, the single self-interstitial ($I_1^{(001)}$) and a form of the di-interstitial (I_2^{NN}) have been identified with the $R2$ and $R1$ electron paramagnetic resonance (EPR) centers, respectively.^{10,11} Recently, a new EPR center labeled $O3$ has also been suggested to be a small interstitial aggregate.¹² The $O3$ data gave rise to two models, one of which is made up from two interstitials and one being a tri-interstitial. It is by no means clear from the published data that a conclusive model for $O3$ has been established.

The assignments to small aggregates of interstitials have come chiefly from magnetic resonance investigations. The spin Hamiltonian of all of these $S=1$ centers contains an interaction term between two carbon radicals of the form $(S \cdot D \cdot S)$, where the D tensor uniquely identifies the center. In general, the D tensor contains a spin-orbit term. This is

usually small in comparison to that arising from the spin-spin interaction. The point dipole approximation to the D tensor has been taken to imply a separation between C radicals of around 2.8 Å in the case of $R2$. It was this large estimated separation that led to the original assignment to a divacancy or di-interstitial.⁴² When approximate allowance for the distributed spin density is made,¹¹ this separation drops to 1.5 Å. However, this separation is still considerably greater than the 1.26 Å found for $I_1^{(001)}$ in previous *ab initio* (AIMPRO) modeling,¹³ and 1.27 Å calculated by Li and Lowther¹⁴ using a different approach. Thus the assignment of $R2$ to the single interstitial is not without problems. However, we show that a detailed calculation of the D tensor resolves this controversy.

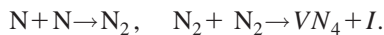
In this paper we again use AIMPRO to investigate the structure and electronic properties of interstitial defects, but extend the method to compute the D tensor. Previously, AIMPRO has been used to analyze the vibrational modes of nitrogen aggregates,¹⁵ vacancy-nitrogen, vacancy-silicon,¹⁶ and vacancy-phosphorus¹⁷ defects with conspicuous success. Section II A describes the general method employed, and specifically the way the D tensor is calculated.

Important information on interstitial defects also comes from optical studies. Three absorption peaks at 1.685, 1.859, and 3.9 eV have been correlated with $R2$, viz., the single interstitial.^{11,18,19} However, other workers²⁰ have assigned a different optical line to I_1 . This is the $3H$ band at 2.46 eV which is observed directly following electron irradiation and survives annealing²⁰ to 670 K, and may be stable up to 900 °C.²¹ The local mode replicas indicate an interstitial-related defect, and recent annealing experiments suggest that its intensity increases when the $R2$ and $R1$ defects begin to anneal out.²² The assignments for these optical features are

discussed in Secs. III and IV where the theoretical optical properties of the single and di-interstitials are described in detail. We do not find that the optical properties of I_1 closely match $3H$ and instead suggest that $3H$ is linked with a structural form of I_2^{NN} distinct from the $R1$ EPR center.

The favored structure for the single interstitial has long been taken to be a $[001]$ split interstitial.^{13,23} This defect has two dangling bonds (or unsaturated atoms) at its core. A characteristic feature of the multi-interstitial defects is that the number of dangling bonds per interstitial is reduced through reconstruction. This provides the binding energy for the centers and is the driving force for the aggregation process. Spin-1 centers usually arise from a coupling of two radicals, and $I_1^{(001)}$ and I_2^{NN} are examples where the defects possess exactly two dangling bonds. Now, we have found only one way to combine three split interstitials to produce a spin-1 defect with two dangling bonds, and in Sec. V A the D tensor for this form of I_3 is found to be almost identical to that measured for the $O3$ EPR center. This gives corroborating evidence with which to identify I_3 with the $O3$ center. The structure of I_3 strongly implies that a form of I_4 in which all dangling bonds are removed is a particularly stable defect and is likely to be formed when $O3$ anneals out. This is important because it in turn suggests that a stable extended defect can arise from the aggregation of I_4 defects onto a single $\{001\}$ plane. This provides a clue to the structure for the platelet, detected in many natural type Ia diamonds, or type Ib diamonds that have been annealed for long periods at temperatures above 2400 °C.²⁴

Heat treatment of type Ib diamond is thought to create interstitials by the aggregation of nitrogen: single substitutional nitrogen defects combine into dimers (A centers), which are subsequently combined into vacancy-nitrogen defects (B centers) with the release of $I_1^{(001)}$,^{25–27} i.e.,



The nitrogen content within the platelets varies; however, platelets form only in material where nitrogen aggregates. Specifically, irradiation and annealing do not produce these extended structures. The role of nitrogen is not fully understood. Models of platelets consisting of an array of I_4 units have been proposed previously as a result of transmission electron microscope (TEM) studies but without detailed theoretical support. Here, we demonstrate that the platelet gives a displacement of $[001]$ planes which increases from $0.3a_0$ for a single I_4 defect to $0.4a_0$ for an infinite plane of I_4 defects. These values are in agreement with TEM measurements. We calculate that the I_4 model also gives vibrational bands that are consistent with the B' vibrational band attributed to platelets. This band correlates linearly with the number of B centers in so called regular natural diamonds²⁵ lending weight to the interstitial model of the platelet. Thus the calculations give a good account of the stages of interstitial aggregation from point to extended defects.

Nevertheless, there are some unexpected findings. The most important of these is that the observed spin-1 I_2 and I_3 defects are not the lowest-energy structures: there are other, diamagnetic configurations that are considerably lower in en-

ergy. In some cases, e.g., I_3 , the diamagnetic center may be difficult to form as a substantial barrier may have to be overcome. In others, e.g., I_2^{NN} , we argue that a second form of the defect is a prominent optical center labeled $3H$. Nevertheless, these alternative forms may be separated by a substantial barriers so that they coexist in the diamond. Thus, to date only paramagnetic self-interstitial defects have been properly characterized, leaving a vacuum in the understanding of interstitial aggregation. We discuss these models in Secs. III–V and finally give our conclusions in Sec. IX.

II. METHOD

We use a local spin-density functional method, AIMPRO, in supercells or large H-terminated clusters.^{28,29} Each interstitial defect is modeled by placing the appropriate number of extra carbon atoms into the center of a cluster or supercell. The atom positions are then optimized via a conjugate-gradient algorithm subject to a symmetry constraint, where appropriate.

Hydrogen-terminated diamond clusters of composition ranging from $\text{C}_{71+n}\text{H}_{60}$ to $\text{C}_{184+n}\text{H}_{120}$, where n is the number of interstitial atoms, were employed in this study. The wave-function basis consists of independent s , p_x , p_y , and p_z Gaussian orbitals with four different exponents, sited at each C site. A fixed linear combination of two Gaussian orbitals is sited on the terminating H atoms. In addition, a set of s and p Gaussian orbitals is placed at each C-C bond center. The charge density is fitted with four independent s Gaussian functions with different widths on each C atom and three on the terminating H atoms. One extra s -Gaussian function is placed at each C-C bond center.

Supercell calculations were carried out in cells consisting of $(64-128)+n$ atoms, using an MP-2³ set of \mathbf{k} points to sample the band structure.³⁰ Unit cells were constructed using either the eight-atom conventional unit cell (giving rise to 64-, 96-, and 128-atom unit cells) or four-atom orthorhombic unit cells with lattice vectors along $[110]$, $[\bar{1}\bar{1}0]$, and $[001]$ in the case of most platelet calculations. The basis consisted of four Gaussian s and p orbitals with optimized exponents. One such Gaussian is sited at each bond center. The charge density is Fourier transformed using plane waves with an energy cutoff of 120 Ry. Details of the method have been given previously.²⁹

In general, the results for the structure and energies of defects found using the cluster and supercell methods are similar. Each method has its own advantages. The cluster method is faster and the ionization energy and electron affinity can be easily evaluated, giving information on the electrical activity of defects.³¹ On the other hand, the supercell method is to be preferred for properties such as diffusion energies since these quantities are independent of the location of the defect within the supercell.

The theory employed strictly fails for excited state properties of a system, and hence for excitation processes. This is true independent of the choice of clusters or supercells. One can approximately calculate direct excitation energies using theories such as that due to Slater.³² Specifically, the excitation between two localized states—which is often the case in

diamond—gives a reasonable agreement with experiment. For optical transition energies in other materials, such as silicon, one gains a good understanding based on the electronic properties (donor and acceptor levels) of a given defect. This information comes from the ionization potential and electron affinity which are both ground state properties and hence accessible by local density functional theory.

A. The D tensor

The dipole contribution to the spin-spin interaction tensor is given by:

$$D_{ij} = \frac{\mu_0 g^2 \beta_e^2}{8\pi} \int d\mathbf{r}_1 d\mathbf{r}_2 \rho(\mathbf{r}_1, \mathbf{r}_2) \times \left\{ \delta_{ij} - 3 \frac{(r_{1i} - r_{2i})(r_{1j} - r_{2j})}{|\mathbf{r}_1 - \mathbf{r}_2|^2} \right\} |\mathbf{r}_1 - \mathbf{r}_2|^{-3}. \quad (1)$$

Here β_e is the Bohr magneton, g the electron Landé factor, and ρ the probability of locating spins at points \mathbf{r}_1 and \mathbf{r}_2 . D_{ij} is a two-particle correlation function and cannot be found from the spin densities. This type of approach has previously been used for spin-1 centers.³³ We assume that ρ is determined from the two electrons occupying the two highest spin-up Kohn-Sham orbitals λ and μ . The expression for ρ is then

$$\rho(\mathbf{r}_1, \mathbf{r}_2) = |\Psi(\mathbf{r}_1, \mathbf{r}_2)|^2, \quad (2)$$

$$\Psi(\mathbf{r}_1, \mathbf{r}_2) = \frac{1}{\sqrt{2}} \{ \psi_\lambda(\mathbf{r}_1) \psi_\mu(\mathbf{r}_2) - \psi_\lambda(\mathbf{r}_2) \psi_\mu(\mathbf{r}_1) \}. \quad (3)$$

Consider the case, relevant here, that μ and λ are localized on two C radicals with separation R . When R is much larger than the localization length³⁴ for each orbital, then the exchange term can be ignored, and the point dipole expression for D becomes

$$D_{ij}^a = \frac{\mu_0 g^2 \beta_e^2}{8\pi} \left\{ \delta_{ij} - 3 \frac{R_i R_j}{R^2} \right\} / R^3. \quad (4)$$

The matrix D^a has three principal values,

$$D_1^a = D_2^a = -D_3^a/2 = \frac{\mu_0 g^2 \beta_e^2}{8\pi R^3}.$$

D_3^a is directed along the line joining the radicals. This formula has often been used but seriously overestimates R , as the distributed nature of the spin density is ignored. In this study, we compute the integral in Eq. (1) both analytically and numerically using the wave functions obtained from the calculations. Both methods give almost identical results. The theory here neglects spin-orbit contributions which are thought to be small for diamond.

The convergence of the defect structures and D tensors was tested with respect to both cluster size and surface treatment. Relaxation of the terminating hydrogen of the cluster containing the largest defect, I_4 , gave rise to shifts of less than 3% in the bond lengths. Similarly, the magnitudes of

the D -tensor elements of I_3 were found to vary by less than 2% with surface relaxation. Increasing the cluster size from $C_{72}H_{60}$ to $C_{183}H_{115}$ resulted in variations in the bond lengths of $I_1^{(001)}$ of under 1% and a change to the D tensor of less than 2%. This shows that the clusters employed in this study are large enough to provide us with structures and electronic properties that are not affected by the surface condition to within the accuracy of the method.

B. The B tensor

The energy E of an anisotropic defect such as $I_1^{(001)}$ in an externally imposed strain field depends on the orientation of the defect with respect to the strain field. This dependence is expressed through the stress energy or piezospectroscopic B tensor³⁵ $E = \text{tr}(B \cdot \epsilon)$ where ϵ is the strain tensor and B is a traceless symmetric tensor that is readily calculated from a strained supercell.²⁹ Both the volume of the cell and the atomic positions are first relaxed to ensure that the tensor is traceless, and then strains are imposed across the surfaces of the supercell. The atomic positions are then relaxed a second time and the change in the energy found. The derivative of the energy change with strain is then the B tensor. The tensor can be experimentally measured by imposing a uniaxial stress on the crystal and determining the equilibrium fraction of defects aligned along the stress axis. The tensor does not depend on any barrier between different orientations.

C. Optical transitions

The energies for optical transitions are found from the cluster method ($C_{72}H_{60}$) using Slater's transition-state method³² together with Janak's theorem. These relate the absorption energy to the difference in Kohn-Sham levels of a configuration where half an electron is promoted from one Kohn-Sham level to another. The cluster method usually, and accidentally, gives a band gap energy around 5 eV, which is close to the fundamental gap of diamond. This is due to the surface hydrogen atoms as the supercell technique, with a similar basis, gives direct and indirect band gaps of 5.58 and 4.17 eV, respectively, very close to those from other local density approximation calculations.³⁶ Typically the cluster method estimates optical excitation energies of defects to within about 25%. The radiative rates of the transition are related to the dipole matrix elements which can be evaluated using the pseudo wave functions corresponding to each level.¹⁶

D. Vibrational modes

Vibrational modes are calculated by the diagonalization of a dynamical matrix found from the numerical double derivatives of the total energy between core atoms of the defect. Matrix elements of other atoms are found from a valence force potential given previously.³⁷ The local vibrational modes are typically within about 10% of experiment, but the method becomes less reliable for modes lying close to or below the Raman frequency.

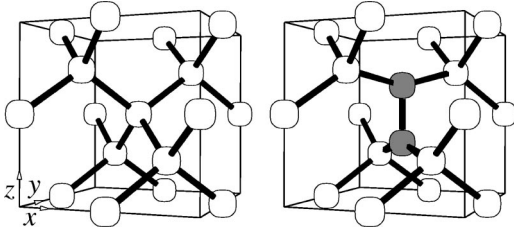


FIG. 1. Schematic picture of [001]-oriented split interstitial $I_1^{(001)}$. A section of defect-free material is also shown for comparison.

III. THE SINGLE SELF-INTERSTITIAL I_1

Previous AIMPRO calculations¹³ have shown that the stable neutral interstitial has spin equal to zero and a structure derived from a slightly distorted [001]-oriented split interstitial. The distortion lowered the ideal D_{2d} symmetry (Fig. 1) to D_2 , resulting in a calculated energy drop of around 0.6 eV. When constrained to D_{2d} symmetry, the two dangling-bond orbitals lie perpendicular to each other along $[110]$ and $[\bar{1}\bar{1}0]$ and the carbon radicals are separated by 1.26 Å. These degenerate p orbitals give rise to a half-filled e doublet in the upper half of the Kohn-Sham eigenspectrum while an a_1 level lies close to the valence band edge. An $S=1$ state (which retains D_{2d} symmetry) was found to lie about 0.5 eV above the ground state. These properties are qualitatively consistent with those of the $R2$ EPR center linked to the interstitial.¹¹ $R2$ is a spin-1 center with tetragonal symmetry observed directly following e irradiation of type IIa diamond (containing low concentrations of impurities) at room temperature. Hyperfine measurements show that the unpaired wave function is localized on two equivalent atoms. However, the temperature dependence of $R2$ shows that the triplet state lies only 50 meV above the ground state. This is much smaller than the theoretical estimate given earlier and we have now recalculated this energy difference using an updated code.

The D_{2d} , e^2 configuration leads to four many-body states: 1B_1 , 3A_2 , 1A_1 , and 1B_2 . Labeling the e orbitals x and y , approximate many-body wave functions can be written as

$$\begin{aligned}\Psi(^1A_1) &= [x_1x_2 + y_1y_2][\uparrow\downarrow - \downarrow\uparrow], \\ \Psi(^1B_2) &= [x_1x_2 - y_1y_2][\uparrow\downarrow - \downarrow\uparrow], \\ \Psi(^1B_1) &= [x_1y_2 + y_1x_2][\uparrow\downarrow - \downarrow\uparrow], \\ \Psi(^3A_2) &= [x_1y_2 - y_1x_2] \left\{ \begin{array}{l} [\uparrow\uparrow] \\ [\uparrow\downarrow + \downarrow\uparrow] \\ [\downarrow\downarrow] \end{array} \right\}.\end{aligned}$$

The energies of these multiplets can be found using the von Barth procedure³⁸ where each Slater determinant is written as a linear combination of multiplet wave functions. The $S=1$ state is simply given by $|x^\uparrow y^\uparrow\rangle$. The energy of the $|x^\uparrow y^\uparrow\rangle$ state is the average of the 3A_2 and 1B_1 states and thus the energy of the 1B_1 state can be found. Unfortunately, one

cannot divide the remaining multiplets, and the $|x^\uparrow x^\uparrow\rangle$ determinant gives only the average of the 1A_1 and 1B_2 states. The present calculations place 1B_1 about 10 meV below 3A_2 and around 1.4 eV below the average energy of the 1A_1 and 1B_2 states. Thus these calculations account for the small difference in the singlet and triplet states provided that the singlet state is not lowered significantly in energy by a symmetry distortion. We shall show later in the paper that this is in fact the case for the present calculations, in contrast to the previous calculations.¹³

The migration path for $I_1^{(001)}$ involves the reorientation of the split interstitial from (say) [001] to [010]. The barrier to migration has previously been calculated to be 1.7 eV.¹³ This value is in good agreement with the experimental barrier of 1.6–1.7 eV determined from the loss of vacancies at around 700 K, presumably through interstitial-vacancy recombination.^{39,40} This agreement adds further support to the assignment of $R2$ to $I_1^{(001)}$.

The split interstitial structure compresses the lattice along [001]. The resulting stress can be quantified in terms of the piezospectroscopic stress-energy B tensor described in Sec. II B. The D_{2d} symmetry reduces the number of independent components of the B tensor to one, so $B_3 = -2B_1 = -2B_2$, with the principal directions lying along the cube axes. We have calculated the value of B_3 in 65- and 97-atom cubic supercells, finding -28 and -29 eV, respectively. The tensor can be measured by applying stress to the crystal and determining the equilibrium fraction of defects aligned along each cube axis. Reference 11 gives the relative populations of the orientations of $R2$ under stress, from which we estimate $B_3 = -24$ eV, in excellent agreement with the calculated value. This gives strong support to the assignment and implies that the calculated separation of 1.26 Å between the radicals must be largely correct.

A remaining problem with the assignment is the small measured values of the D tensor. Applying the point dipole expression discussed in Sec. II A gives a separation between the two carbon radicals of 2.8 Å. This is almost *twice* the calculated value. The effect of a spin-density distribution decreases this separation and a crude estimate gives 1.5 Å.¹¹ However, this value is still significantly larger than the calculated one. We have therefore used AIMPRO to derive the dipole-dipole contribution to the tensor.

Substituting the Kohn-Sham e^\uparrow orbitals into Eq. (3) generates the D tensor [Eq. (1)] and Table I gives its principal values and directions. Thus D_3 is found to be -1.82 GHz compared with an experimental value of ± 2.78 GHz.^{41,42} The sign has not been determined experimentally. Our calculated value *underestimates* the magnitude of the tensor by a factor of only 0.65 whereas the point dipole approximation would overestimate its magnitude by a factor of 8. This shows that the small D tensor is to be understood as coming from a diffuse spin density. The underestimate may be the result of deficiencies in the theory or of the neglect of the spin-orbit contribution.

We have examined carefully the sensitivity of the tensor to the details of the calculation. Using a variety of bases, we find that the principal component of the D tensor varies by

TABLE I. The calculated and experimental principal values (GHz), in descending order, and principal directions $[n_1 n_2 n_3]$ for the spin-spin tensor D . In each case n_3 is almost parallel to the vector joining the radicals.

	$R(\text{\AA})$	D_1	D_2	D_3	n_1	n_2	n_3
$I_1^{(001)}$: Calc.	1.28	0.91	0.91	-1.82	$[1 \ 1 \ 0]$	$[1 \ 1 \ 0]$	$[0 \ 0 \ 1]$
$R2$: Expt. ^a		± 1.39	± 1.39	∓ 2.78	$[1 \ \bar{1} \ 0]$	$[1 \ 1 \ 0]$	$[0 \ 0 \ 1]$
I_2^{NN} : Calc.	1.81	1.19	0.78	-1.97	$[1 \ \bar{1} \ 0]$	$[0.21 \ 0.21 \ 0.95]$	$[0.67 \ 0.67 \ -0.30]$
$R1$: Expt. ^b		1.41	1.40	-2.81	$[1 \ \bar{1} \ 0]$	$[0.21 \ 0.21 \ 0.95]$	$[0.67 \ 0.67 \ -0.30]$
I_3 : Calc.	3.62	0.40	0.29	-0.69	$[1 \ 0 \ 0]$	$[0.0 \ 0.31 \ 0.95]$	$[0.0 \ 0.95 \ -0.31]$
$O3$: Expt. ^c		0.46	0.35	-0.81	$[1 \ 0 \ 0]$	$[0.0 \ 0.31 \ 0.95]$	$[0.0 \ 0.95 \ -0.31]$

^aReference 41.

^bReference 10.

^cReference 12.

$\sim 5\%$. In general, for the single interstitial additional basis functions tended to increase the magnitude of the D -tensor elements, although this is not true for the other defects considered. We have also examined the variation with cluster size. Clusters of the form $C_{72}H_{60}$, $C_{88}H_{77}$, and $C_{183}H_{115}$ give values of D_3 that vary by only $\sim 3\%$. These figures have proved consistent across the range of $S=1$ centers in diamond we have thus far examined. This demonstrates that the D tensor is not sensitive to the precise form of the orbitals. In spin-polarized theory, the empty e^\downarrow orbitals are different from the filled e^\uparrow . However, using these spin-down orbitals yields D_3 as -1.91 GHz—indicating again only a few percent difference.

In summary, application of the point dipole approximation leads to a D tensor much greater than the experimental value. This has been a problem for the assignment of the $R2$ center to a single interstitial but the present calculations show that the discrepancy can be explained by a distributed spin density. A general conclusion is then that the point dipole approximation is inadequate in describing centers where the inter-radical separation is small.

A. Optical properties

In contrast to the magnetic properties, the optical properties of the defect are complicated and are not completely understood. $R2$ has been correlated with three optical transitions seen in absorption,^{11,18,19} whose peaks are at 1.685, 1.859, and 3.9 eV. The symmetry of the optical center has been described as tetragonal.¹⁸ The 1.685 eV peak is a transition between excited states as it disappears at very low temperatures. The temperature dependence of this line suggests that absorption occurs from a state about 6 meV above the ground state energy. Recent experiments examining the dependence of the peak position on the carbon isotope mixture⁴³ suggest that the 1.859 eV transition is a one-phonon replica of a *dipole-forbidden* transition. The 1.685 and 1.859 eV transitions share an excited electronic state.⁴³

We assign an $a_1 \rightarrow e$ single-particle transition (see Fig. 2) to the 3.9 eV ($R11$) optical transition. In terms of multiplets, this ${}^1B_1 \rightarrow {}^1E$ transition is dipole allowed. Using the Slater transition-state method, we estimate its energy to be 4.3 eV, in good agreement with experiment. The radiative lifetime is

calculated at around 50 ns, which to our knowledge has not been measured. The location of the ground and excited states with reference to the bands has not been ascertained from the calculation, and it is possible that the excited state is resonant with the conduction band. This would tend to increase the lifetime. However, the absorption peak is fairly sharp,¹⁹ suggesting that the excited state is in the band gap. The absence of a luminescence corresponding to $R11$ remains to be explained.

Understanding the other two optical transitions is not so straightforward, however.

The calculations discussed above find that the separation between multiplets is of the order of the 1.685 and 1.859 eV transitions, and thus these transitions are thought to be internal ones between these multiplets. In contrast with the 3.9 eV transition, no other configurations are involved. Now, the lowest-energy $S=0$ state in D_{2d} has 1B_1 symmetry and dipole transitions to the 3A_2 , 1B_2 , and 1A_1 states are forbidden, as only transitions to 1A_2 states are allowed. This lack of an allowed optical transition out of the ground state is in agreement with the optical data. It appears then that the state lying 6 meV above the ground must be either 1B_2 or 1A_1 . The allowed optical transition at 1.685 eV should correspond to a transition between these as dipole transitions to 3A_2 are

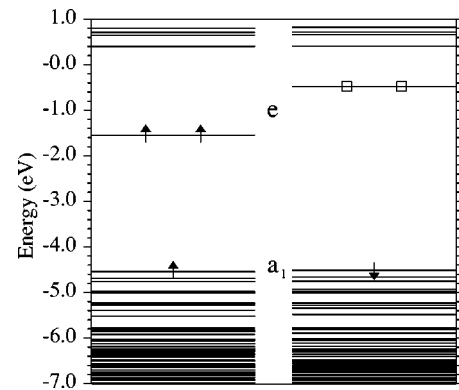


FIG. 2. Spin-polarized Kohn-Sham levels for the D_{2d} [001]-oriented split interstitial; spin-up levels are shown on the left, spin-down on the right. Filled levels in the vicinity of the band gap are indicated by arrows, and empty levels by empty squares. The highest occupied level is a doubly degenerate e level.

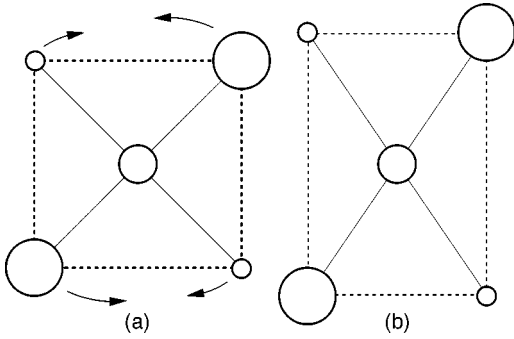


FIG. 3. An illustration of the dynamic perturbation of I_1 in the ground state. (a) shows the view down the principal C_2 axis of the D_{2d} structure. The atom radii indicate depth. The curved arrows indicate the sense of the twist leading to one of the two equivalent D_2 symmetry structures shown in (b).

forbidden. However, there is no reason to believe that the 1A_1 or 1B_2 multiplets lie within 6 meV of the 1B_1 ground state. If indeed one of these states is almost degenerate with the ground, then according to our calculations above the other state lies at around 2.8 eV, which is far from the observed transition energy.

Davies *et al.*⁴³ have recently suggested that the 6 meV excited state arises from the interaction of the ground and lowest $S=0$ excited states, which attempt to cross each other as a result of a structural distortion. In the absence of distortion where the defect has D_{2d} symmetry, the excited state is 230 ± 50 meV above the ground state. Our difficulty with this model is again the unlikely event that the 1A_1 or 1B_2 multiplets lie around 0.23 eV above the ground state. We therefore present a model below where the 6 meV splitting comes from the coupling of two symmetrically equivalent distortions and is similar to inversion doubling in the ammonia molecule.

Now, it has been found previously¹³ that, in the $S=0$ spin state, the interstitial can undergo a symmetry lowering distortion to D_2 , as indicated schematically in Fig. 3. This distortion involves a clockwise (or counterclockwise) twist about the principal axis, and attempts to align the two dangling bonds on the two C radicals, leaving the bond lengths unchanged. Thus an element of π bonding is introduced, stabilizing the distortion and splitting the e level into b_2 and b_3 . In a one-electron picture, this is identical to a Jahn-Teller effect. The perturbation is not large, and the stable structure leads to an angle between the two C dangling bonds that differs from D_{2d} by only 3.3° . The configurations $b_2^{\uparrow\downarrow}$, $b_2^{\uparrow}b_3^{\downarrow}$, $b_2^{\downarrow}b_3^{\uparrow}$, and $b_3^{\uparrow\downarrow}$, lead to states of 1A , 3B_1 , 1B_1 , and 1A symmetries in D_2 and yield the energies shown in Fig. 4 as a function of the distortion. The calculation does not include any electron interaction beyond that present in local density functional theory and, in particular, the two 1A states would tend to be split apart further by the interaction for smaller distortions. The dashed lines indicate speculated energies where this interaction is included. At the D_{2d} limit the sum of the 1A and 1B energies would be that generated from the von Barth analysis, viz., 1.4 eV, and the 3A_2 and 1B_1 states become almost degenerate. The points at the very right

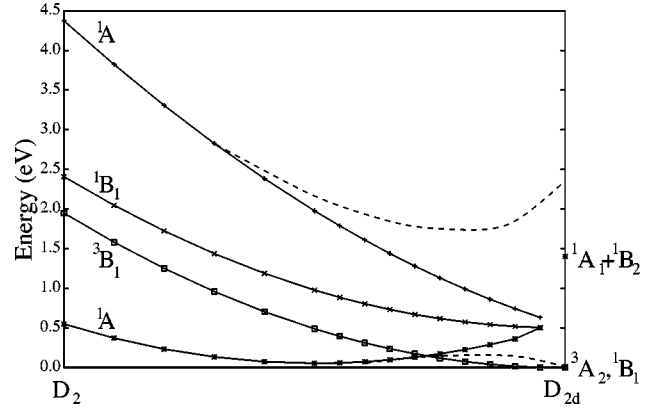


FIG. 4. Plot of the calculated energies of the multiplets of neutral $I_1^{(001)}$ as a function of a D_2 distortion (see Fig. 3), as discussed in the text. The stable distortion corresponds to a 3° twist, and the largest distortion to 7° .

hand side are placed at the energies calculated in D_{2d} using the von Barth approach. Figure 4 also suggests that there is no electronic level close to the ground state as required by Davies *et al.*⁴³

One notes that the distortion energy is very small (in contrast to Ref. 13) and the singlet ground state remains close to the triplet in agreement with experiment. With the uncertain exception of the highest state, the distortion is stable only in the ground state. There are two equivalent distortions involving a clockwise or counterclockwise twist of the defect about [001]. States corresponding to each minimum will be coupled and split by tunneling, leading to two states with effective D_{2d} symmetry in the same way as inversion doubling in the ammonia molecule. These states correspond to bonding and antibonding combinations of wave functions centered at each of the distorted D_2 structures. They have symmetries 1B_1 and 1A_1 , respectively, and we suppose that they are split by 6 meV. We can now understand the optical properties of the center. The ground state is 1B_1 from which no dipole-allowed optical transitions can occur. The 1A_1 state 6 meV higher in energy permits a transition to the 1B_2 state, and we place this at 1.691 eV above the ground state. Finally a one-phonon replica between the ground state and 1B_2 accounts for the 1.859 eV band. The various transitions between these states are sketched in Fig. 5.

The $^1B_1 \rightarrow ^1B_2$ transition is forbidden in agreement with observation. It can be rendered active by coupling with a local mode of the correct symmetry. This must be B_1 or E for in a dipole-allowed transition

$$\Gamma^{\Psi_0} \otimes \Gamma^{\mathbf{p}} \otimes \Gamma^{\Psi_1} \otimes \Gamma^{\chi_p} \supset A_1. \quad (5)$$

The calculated (quasiharmonic) modes for the neutral defect in D_{2d} symmetry are listed in Table II. The lower-energy modes are spread over several atoms. Given the rather poor way in which such bulklike modes are modeled in these calculations, the B_1 mode can be considered to be in tolerable agreement with the observed 169 meV (1363 cm^{-1}). Significantly, the B_1 mode also corresponds to a twisting motion about the principle C_2 axis. A further

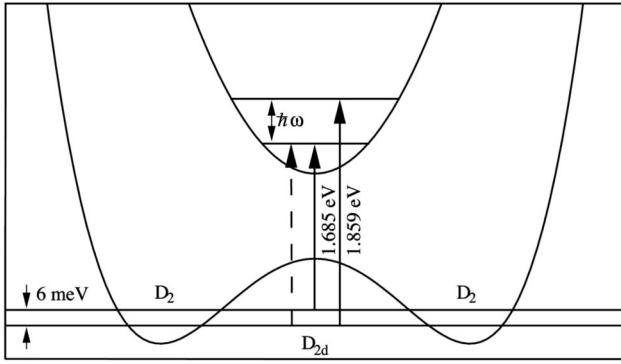


FIG. 5. Postulated configuration coordinate diagram for ground and lower $S=0$ excited states for $I_1^{(001)}$ as a function of the two equivalent D_2 distortions. The ground and 6 meV excited states are made from bonding (1B_1) and antibonding (1A_1), respectively, linear combinations of the ground states of the two D_2 -distorted structures. Full vertical arrows show allowed optical transitions to the excited 1B_2 state; dotted vertical arrow shows forbidden optical two-phonon transition.

consequence is that a two-phonon transition involving this mode would be forbidden, in agreement with the lack of a two-phonon transition in experiment despite the strong one-phonon peak.

In summary, the model where the ground state of $I_1^{(001)}$ involves tunneling between clockwise and counterclockwise twists appears to be consistent with the experimental data for the 1.685 and 1.859 eV bands. Thus it appears that the theory can describe the unusual optical properties of the center although a detailed quantitative prediction is lacking. Our model differs from that of Davies *et al.* in two major ways. First, we do not have to have two states close in energy to derive the 6 meV splitting. Secondly, we make a prediction of the symmetry of the local mode involved in the 1.859 eV transition that can be experimentally tested.

B. Summary

To summarize, a number of independent properties ascribed to the single self-interstitial have been explained using theory. These include the optical behavior, D tensor, piezospectroscopic data, and annealing properties. For a model to be accepted, it must explain all of the observations, not just one or two. It is a clear strength of the method employed in this study that so many points of agreement are made.

TABLE II. Local vibrational modes and their symmetries of the D_{2d} single self-interstitial (cm^{-1}). For the mixed isotope case, one of the central atoms has been replaced by ${}^{13}\text{C}$.

${}^{12}\text{C}$ (D_{2d})		${}^{12}\text{C}/{}^{13}\text{C}$ (C_{2v})		${}^{13}\text{C}$ (D_{2d})	
1915	A_1	1842	A_1	1840	A_1
1516	E	1516	B_1	1456	E
		1487	B_2		
1333	B_2	1331	A_1	1281	B_2
1322	B_1	1322	A_2	1270	B_1

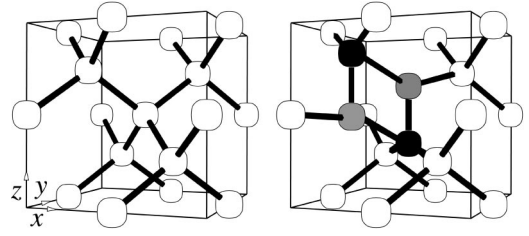


FIG. 6. Schematic picture of the di-[001] split-interstitial model for $R1$. Threefold interstitial atoms are indicated in gray and fully coordinated interstitial atoms in black. A section of pure diamond is shown for comparison.

IV. THE DI-INTERSTITIAL

We now consider the di-interstitial I_2 . We believe there are at least three structural forms of this defect with considerable energy barriers to interconversion, and thus several types can coexist in diamond. We first describe the spin-1 defect that has been found experimentally.

There are two ways in which two [001] split interstitials can be brought together, forming I_2 , which eliminate two of the four dangling bonds. The first consists of two [001] split interstitials at nearest-neighbor (I_2^{NN}) positions (Fig. 6). This structure has been previously proposed as the $S=1$ EPR center labeled $R1$.¹⁰ A second form is shown in Fig. 7, and is similar to the $R1$ center in that it is made up from two [001] split interstitials, has planar symmetry, and possesses only two dangling bonds. In this case the [001] split interstitials are at next-nearest-neighbor sites, and this structure is commonly referred to as the ‘‘Humble ring’’ (which we shall label $I_2^{2\text{NN}}$). It was first proposed as a building block of the platelet.⁷ We shall return to this structure in Sec. IV B.

A third structure involves bridging two bond-centered interstitials placed across the hexagonal ring.

A. The $R1$ defect

The $R1$ center, which has C_{2h} symmetry, is formed along with $R2$ during room temperature irradiation of chemically pure (type IIa) diamond.^{10,42} Our calculations show that the optimized NN structure possesses C_{2h} symmetry in agreement with experiment and the spin-triplet configuration was found to lie 0.1 eV lower in energy than $S=0$, independent of cluster size. The inter-radical separation is 1.7 Å. The calculated principal directions of the D tensor, which are

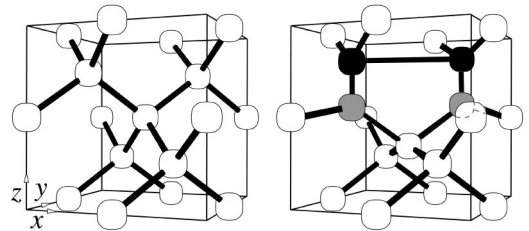


FIG. 7. Schematic picture of the the Humble di-[001] split interstitial. Threefold interstitial atoms are indicated in gray and fully coordinated interstitial atoms in black. A section of pure diamond is shown for comparison.

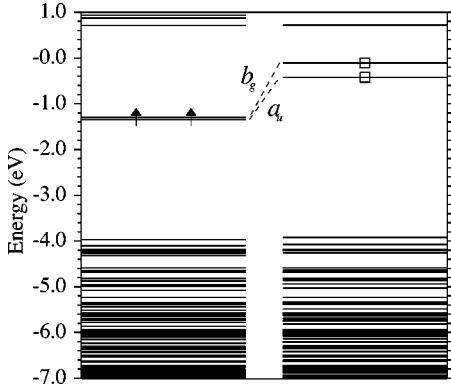


FIG. 8. The spin-polarized Kohn-Sham levels for the $R1$ center. Notation as in Fig. 2. The two highest occupied levels around -1.3 eV have symmetries a_u and b_g . The 1.7 eV optical transition occurs to the next level (a_g symmetry) at 0.8 eV.

listed in Table I, are in excellent agreement with the measured ones, and the values are in fair agreement. It is interesting to note that the experimental D tensor, which is derived by a fit to the data, exhibits axial symmetry, suggesting the applicability of the point dipole approximation so that $D \approx D^a$. This would, however (as for $I_1^{(001)}$) imply an inter-radical separation of 2.6 Å, which is comparable with the separation of second-shell atoms, and far from the calculated separation of 1.7 Å. Thus one must conclude that the point dipole approximation is inapplicable and the spin density is delocalized. The wave function may then be expected to overlap several neighbors and the symmetry of the D tensor to reflect that of the defect. In this case we would not expect D_1 and D_2 to be degenerate. Since the experimental values are nearly equal, we assume D_1 and D_2 are accidentally degenerate as there is no symmetry relation between these principal directions. It may be that the difference in D_1 and D_2 is very sensitive to the details of the wave functions and beyond the accuracy that can currently be achieved. However, the agreement between the calculated and observed principal directions leaves no doubt as to the correctness of the assignment.

The $R1$ center is associated with an optical excitation around 1.7 eV, although the suggested mechanism for the transition is rather complex.⁴⁴ The electronic ground state of the $S=1$ complex is made from the two singly occupied p orbitals perpendicular to the plane of symmetry, and has overall 3B_u symmetry. In the one-electron picture there are two levels deep in the gap, with b_g and a_u symmetry, lying below an unoccupied level of a_g symmetry (see Fig. 8). A transition-state calculation gives an optical transition at around 1.76 eV in close agreement with the 1.7 eV threshold of Ref. 44. Multiplets formed from the configuration $a_u^n b_g^m (n+m=2)$ have energies within 1 eV of the ground state, and are unlikely to account for the experimental observation. There are two main reasons why dipole-allowed transitions may not be observed in absorption. The first is that they are very inefficient, that is to say, the absorption coefficient is very small. The second is that the energy of the transition is in a technically difficult region of the spectrum

TABLE III. Local vibrational modes and their symmetries of the di-interstitial models (cm^{-1}). A_u and B_u modes in C_{2h} , and all modes except A_2 in C_{2v} , are IR active.

NN (C_{2h})		2NN (C_{2v})		(2NN) ⁺ (C_{2v})		π -bond (C_{2h})	
1978	A_g	1842	B_2	1820	B_2	1961	B_g
1886	B_u	1826	A_1	1813	A_1	1958	B_u
1584	B_u	1594	B_2	1530	B_2	1940	A_g
1549	A_g	1495	A_1	1461	A_1	1577	A_u
1364	A_g	1323	B_1	1333	A_1	1463	B_u
		1313	A_1	1321	B_1	1440	A_g
						1417	A_g

to detect. The high- (≥ 4 eV) and low- (≤ 1 eV) energy regions have relatively little data.

The short C-C bonds in the defect imply high-frequency local vibrational modes which, if the defect is present in sufficient concentrations, should be detectable by infrared (IR) absorption. The frequencies and their symmetries are listed in Table III. The highest mode at 1978 cm^{-1} is infrared inactive and similar to that of $I_1^{(001)}$ (1915 cm^{-1}).

B. The Humble form of I_2

The Humble form of I_2 , consisting of two $[001]$ split interstitials at next-nearest-neighbor sites (I_2^{NN}), has C_{2v} symmetry (Fig. 7). The difference in total energy between the $R1$ and Humble forms using $C_{100}H_{78}$ is small for $S=1$, but the $S=0$ diamagnetic Humble defect is 0.7 eV lower in energy than $R1$. This suggests that, although $R1$ is observed by EPR, another, more stable I_2 exists in a diamagnetic state.

There is some evidence that supports this idea. While the production rates of the neutral vacancy and $R1$ are roughly independent of the irradiation temperature there is a marked drop in the creation of $R2$ at higher temperatures.⁴⁵ Thus at 350 K there are ~ 16 times fewer $R2$ centers produced at a given fluence than at 100 K. The loss of $R2$ could be explained through a preferential formation of, say, the $S=0$ Humble defect.

The migration barrier of I_2 has been calculated by relaxing intermediate configurations with constraints that prevent the structure relaxing into the $R1$ or Humble forms. An intermediate metastable structure was found during this procedure but the saddle point was found to be 1.7 eV for the $S=1$ defect. Thus the thermal barriers to diffusion of $I_1^{(001)}$ and I_2 are roughly equal and this could explain why $R1$ and $R2$ anneal out at approximately the same temperature, ~ 600 K.

C. The $3H$ optical center

$3H$ is an optical center detected after room temperature electron irradiation and is reported to be stable to 670 K,²⁰ but may be stable to 1173 K.²¹ Photoillumination with a UV lamp, or a heat treatment, results in a rapid reduction in its intensity (bleaching), suggesting that the defect responsible is charged. $3H$ possesses several phonon replicas²⁰ the largest of which is shifted from the zero-phonon line by

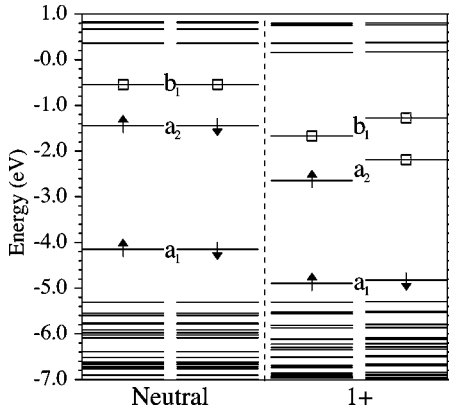


FIG. 9. The spin-polarized Kohn-Sham levels in the region of the band gap for I_2^{2NN} in the neutral (left) and $1+$ (right) charge states. Notation as in Fig. 2. The tops of the valence bands have been aligned to facilitate comparison.

1757 cm^{-1} . This shift corresponds to a vibrational frequency expected from a strengthened C-C bond, supporting the identification with an interstitial defect. This replica splits into three peaks in mixed isotope material, consistent with the view that the C atoms with the strengthened bond are equivalent or nearly equivalent to each other. Other local modes are also observed as replicas and have frequencies of 1365 , 1471 , and 1506 cm^{-1} . Although, these modes roughly agree with the calculated modes of $I_1^{(001)}$ (Table II), it is doubtful whether their symmetries would allow them to participate in luminescence, as commonly only A_1 modes are found to accompany zero-phonon transitions.

Furthermore, uniaxial stress measurements show that the symmetry of the $3H$ defect is C_{2v} (rhombic-I), inconsistent with the D_{2d} (tetragonal) or D_2 (rhombic-II) symmetry found for $I_1^{(001)}$ above (Sec. III). In conflict with another suggestion,⁴⁶ the C_{2v} symmetry of $3H$ also rules out a link with the monoclinic-I A_1 EPR center. The symmetry of $3H$ is, however, consistent with I_2^{2NN} and we argue here that $(I_2^{2NN})^+$ has optical and vibrational properties compatible with those of $3H$.

Figure 9 shows the Kohn-Sham levels for the neutral and charged defect ($C_{73}H_{60}$). The $a_1^2 a_2^2 b_1^0$ ground state configuration⁴⁷ for the neutral center possesses overall 1A_1 symmetry. The a_2 and b_1 states arise from bonding and antibonding combinations of the p orbitals on the two carbon radicals. The a_1 state is essentially a bonding combination of orbitals producing the reconstructed bond.

For the neutral defect, excitations of an electron from the a_1 or a_2 level to b_1 are dipole allowed and have transition energies at ~ 3.5 and 1.0 eV , respectively. These are in poor agreement with the 2.46 eV $3H$ transition, but we cannot rule out this defect as a candidate. However, Fig. 9 shows that in $(I_2^{2NN})^+$ the a_2 and b_1 levels are lowered giving an $a_1 \rightarrow b_1$ optical transition around 3 eV , in closer agreement with experiment. The other possible candidate, $a_1^2 \rightarrow a_2^1$ ($^1A_2 \rightarrow ^1A_1$), is dipole forbidden.

The involvement of I_2^{2NN} can explain the bleaching effect because electrons, created by the illumination, will be

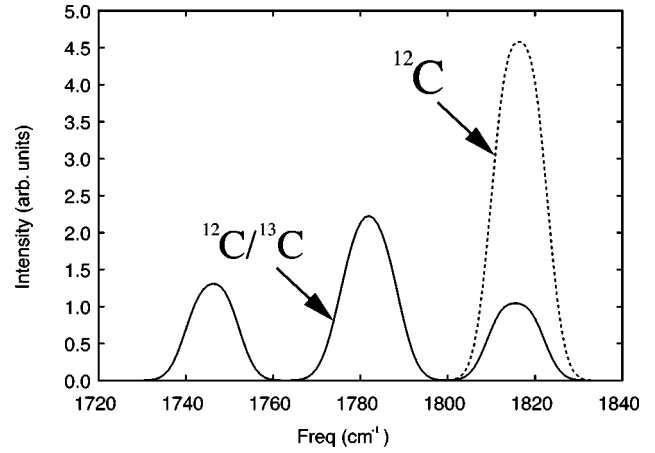


FIG. 10. Intensity (dotted line) of the 1820 and 1812 cm^{-1} bands (^{12}C) for $(I_2^{2NN})^+$. Full curve is intensity in equally mixed ^{12}C - ^{13}C material. Each mode has been Gaussian broadened by 25 cm^{-1} and the height of each peak reflects the number of modes. Note that the mixed spectrum consists of just three peaks with a 1:2:1 ratio of intensities.

trapped by $(I_2^{2NN})^+$ forming I_2^{2NN} . Alternatively I_2^{2NN} could trap a hole to form $(I_2^{2NN})^+$, but, as we shall show below, the neutral defect is metastable and may transform into a more stable optically inactive form.

The donor level of I_2^{2NN} can be estimated by comparing the ionization energy of the defect with that of a defect with a known donor level.³¹ In this case we choose the single substitutional phosphorus center, which is known to possess a donor level at $\sim E_c - 0.6\text{ eV}$.⁴⁸ This gives the donor level of I_2^{2NN} to lie at $\approx E_c - 2\text{ eV}$. In order for the defect to be charged, we require acceptors, for example, vacancies, to be present with levels deeper than this, which seems entirely reasonable. Since $3H$ is also seen in type Ib material, it seems likely that the donor level of the $3H$ defect would be higher than that of substitutional nitrogen ($E_c - 1.7\text{ eV}$), which is consistent within the accuracy of the donor level calculations.

The positive charge state might suggest that the optical center would be present in semiconducting, type IIb diamonds. However, it has been shown that the $3H$ signal is suppressed in this material.²⁰ This may be because either boron self-interstitial complexes are preferentially formed or alternative radiative centers exist.

We note that the assignment of $3H$ to a negative charge state of I_2 is unlikely since we predict that the acceptor level lies at or above the conduction band minimum.

We now discuss the phonon replicas of $3H$. It is usual to assume that the modes detected as phonon replicas have A_1 symmetry if the zero-phonon line is allowed. Table III gives the local vibrational modes of I_2^{2NN} in the neutral and positive charge states. We note that, for the latter, three A_1 modes at 1333 , 1461 , and 1813 cm^{-1} are in fair agreement with the replicas at 1365 , 1471 , and 1757 cm^{-1} . However, the absence of a fourth A_1 mode causes difficulties in assigning the 1506 cm^{-1} replica. However, this is the weakest

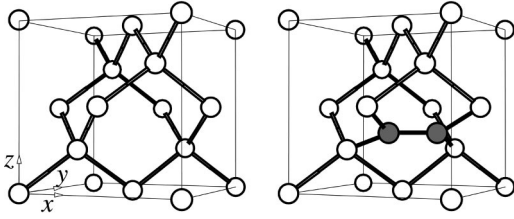


FIG. 11. Schematic of the structure of the low-energy π -bonded di-interstitial. Threefold interstitial atoms are indicated by gray circles. A section of pure diamond is shown for comparison.

transition and might in fact be a combination band involving the B_2 mode at 1530 cm^{-1} as a partner.

The 1820 and 1813 cm^{-1} modes represent out-of-phase and in-phase stretch of the $\langle 001 \rangle$ bonds. The splitting between these modes in pure ^{12}C is only 7 cm^{-1} , implying that the modes are nearly independent vibrations. In the mixed ^{12}C - ^{13}C case, these modes split roughly into five but Fig. 10 makes it clear that only three peaks are to be expected if each mode is broadened by only $\sim 25\text{ cm}^{-1}$. This is consistent with observations on $3H$ in mixed isotopic material, which show that the highest replica is split into three bands, each of width $\sim 25\text{ cm}^{-1}$.²⁰ If only the A_1 mode is considered to couple with the zero-phonon transition, the broadening required to produce only three peaks is reduced.

We have also found that, as the other A_1 modes involve more than two carbon atoms, they do not lead to unique modes split by more than 25 cm^{-1} in mixed isotopic material, in agreement with the observations. The splitting pattern is then consistent with an assignment of $3H$ to the Humble form of $(I_2^{2\text{NN}})^+$.

In summary, we have demonstrated that the positively charged Humble defect has properties compatible with those of the $3H$ optical band. The symmetry of the defect, its vibrational modes, their splitting in isotopically mixed material, and the level structure are in reasonable agreement except possibly for the optical excitation energy itself which is overestimated by 25%. The identification of $3H$ with the Humble form of $(I_2^{2\text{NN}})^+$ demonstrates that a fraction of I_2 species exists in some form other than the spin-1 form of I_2 , identified with $R1$, and naturally explains why the density of $R1$ defects is so much smaller than that of vacancies.^{11,45}

One implication of this assignment is that $3H$ should be correlated with an as yet undetected $S=1/2$ EPR center having C_{2v} symmetry. We also suggest that a measurement of the piezospectroscopic B tensor of $3H$ would provide additional evidence for the Humble model.

D. The π -bonded di-interstitial

We have found another form of I_2 to be competitive in energy. This C_{2h} defect consists of two bond-centered interstitials sited on opposite sides of a hexagonal ring (Fig. 11). The unsaturated p orbitals on the threefold coordinated atoms are perpendicular to the ring and thus can form a π bond. A fully occupied level lies around mid-gap and there do not appear to be any other gap levels. The dipole matrix elements suggest that the $\sim 3.6\text{ eV}$ transition between this

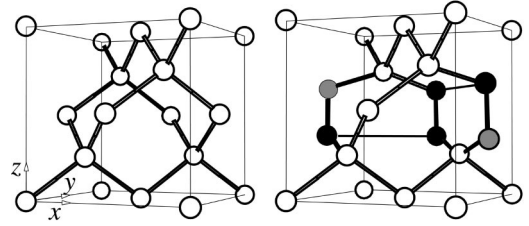


FIG. 12. Schematic picture of the tri-[001] split-interstitial model for the $O3$ EPR center. Threefold interstitial atoms are indicated in gray and fully coordinated interstitial atoms in black. A section of pure diamond is shown for comparison.

level and the lowest empty level near the conduction band has a long lifetime of the order of microseconds. Using $\text{C}_{100}\text{H}_{78}$, in the neutral charge state, the defect has a total energy around 1 eV below the $S=0$ Humble ring, but is 0.26 eV less stable in the positive charge state. Local vibrational modes of the defect are given in Table III.

This structure might be involved in the bleaching of $3H$ as described above. Inter-conversion between the Humble and π -bonded neutral defects can occur provided the activation barrier is sufficiently low. Preliminary estimates of the barrier for interchange between the π -bonded and Humble structures lead to values in the range $1\text{--}1.5\text{ eV}$.

V. THE TRI-INTERSTITIAL

We now consider models for complexes of three self-interstitials.

A. The $O3$ defect

The $O3$, $S=1$ center has C_2 symmetry, appears following e irradiation, and is enhanced by annealing around 600 K when $R1$ and $R2$ disappear. $O3$ anneals out at a temperature only $\sim 50\text{ K}$ higher. This suggests that $R1$ and $R2$ can be precursors of $O3$ and that it anneals out when additional interstitials are added to it. The hyperfine data suggest that the spin density overlaps a unique C atom.

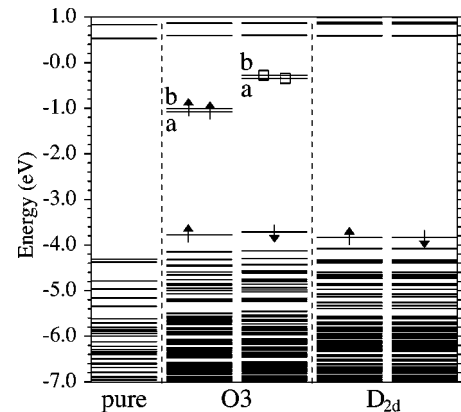


FIG. 13. The spin-polarized Kohn-Sham levels for the $O3$ and D_{2d} models of the neutral tri-interstitial. Notation as in Fig. 2. The Kohn-Sham levels of a defect-free cluster are also plotted.

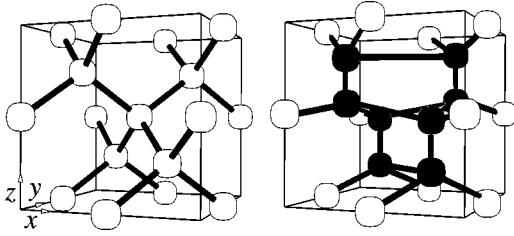


FIG. 14. Schematic picture of the lowest energy structure of the tetragonal tri-interstitial. Threefold interstitial atoms are indicated in gray and fully coordinated interstitial atoms in black. A section of pure diamond is shown for comparison.

A third [001] split interstitial can be added to I_2^{2NN} eliminating two further dangling bonds only if it is located in a different (110) valley (Fig. 12). Four of the six dangling bonds of three isolated $I_1^{(001)}$ centers are eliminated in the construction of this I_3^{2NN} complex, leading to a defect containing a single pair. The relaxed structure has C_2 symmetry, with a unique atom lying between the two radicals. This is consistent with the symmetry and hyperfine structure of $O3$. Categorical support comes from the D tensor calculation using the cluster $C_{187}H_{120}$. Table I shows that the calculated principal values and directions are in close agreement with the measured ones,⁴⁵ giving definitive evidence that $O3$ is this form of I_3 .

The Kohn-Sham levels for the center are shown in Fig. 13. The separation between the two threefold coordinated carbon atoms leads to a modest splitting of the two gap levels, favoring the $S=1$ configuration by around 0.25 eV. There is also the possibility of one or two levels being pushed into the gap just above the valence band top. Thus, the $O3$ center might be correlated with optical activity with excitation occurring between the low-lying levels and those located on the dangling bonds. Such a transition would have an energy in the 3–4 eV region.

B. The tetragonal tri-interstitial

The model for $O3$ is not the lowest-energy structure we have found for I_3 . Placing four [001] split interstitials at sites

TABLE IV. Local vibrational modes and their symmetries of the tri- and tetrainterstitial models (cm^{-1}). All C_2 modes are IR active, whereas only B_2 and E modes are IR active in D_{2d} .

$O3$ (C_2)		I_3 (D_{2d})		I_4 (D_{2d})	
1750	A	1742	A_1	1590	B_1
1742	A	1741	E	1569	E
1627	A	1722	B_2	1534	A_1
1451	A	1416	B_1	1428	A_1
1445	B	1412	A_2	1421	B_2
1398	B	1389	E	1420	E
1393	A	1355	E	1401	B_2
1332	B	1347	A_1	1395	A_1
		1340	A_1	1392	A_2
		1337	A_1	1367	B_1
		1332	E	1362	E
				1349	E

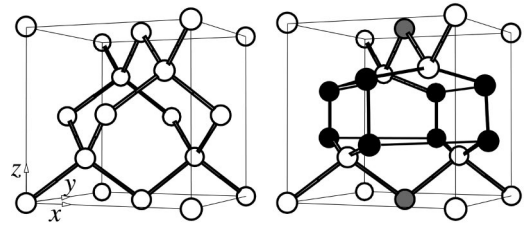


FIG. 15. Schematic picture of the D_{2d} tetrainterstitial. Black atoms indicate the fully coordinated interstitial atoms. A section of pure material is also shown for comparison.

adjacent to a vacancy leads to a fully reconstructed defect with D_{2d} symmetry (Fig. 14) which, in the diamagnetic state, is 1.7 eV lower in energy than $O3$, as calculated using unit cells made up from 96 atoms plus the three interstitials. Figure 13 shows that the defect is electrically and optically inactive. Table IV gives its local vibrational modes along with those of $O3$.

Although this defect has a lower energy, it may be difficult to form or diffuse rapidly. Moreover, it may be the case that the temperatures required to overcome an activation barrier for $O3$ to convert to this lower-energy structure are higher than for the creation of I_4 .

VI. THE TETRAINTERSTITIAL

The $O3$ tri-interstitial structure suggests the structure of the I_4 defect. The addition of one further [001] split interstitial to I_3^{2NN} results in the D_{2d} defect shown in Fig. 15. Here, all dangling bonds have been eliminated and the binding energy of the four $I_1^{(001)}$ defects corresponds to the loss of eight dangling bonds, or a saving of about 27 eV, which is equivalent to 3.4 eV per dangling bond. The bond lengths and angles in the defect are close to ideal. However, a residual strain must exist as a single, fully occupied, defect level lies just above the valence band top (Fig. 16). Although the location of the valence band top is not well defined, we can say that the level is in the band gap since the wave function is relatively localized on the central atoms, and the energy of the level is above that of the highest occupied level

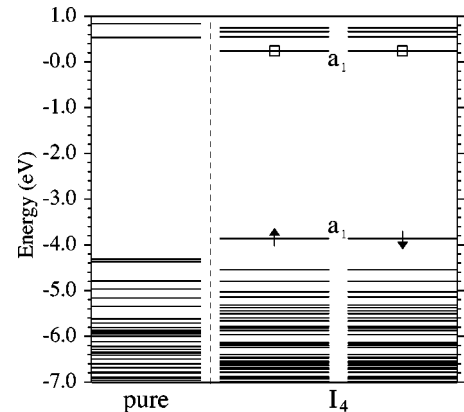


FIG. 16. The spin-polarized Kohn-Sham levels for the neutral tetrainterstitial in diamond. Notation as in Fig. 2. The Kohn-Sham levels of a defect-free cluster are also plotted.

TABLE V. Formation and binding energies relative to single interstitials (eV) as defined in the text for the neutral charge state.

	$I_1^{(001)}$		I_2		I_3		I_4
	NN	2NN	π bond	O3	D_{2d}		
No. dangling bonds	2	2	2	0	2	0	0
E^f	12.3	18.7	18.0	16.9	23.5	21.6	21.9
E^f per interstitial	12.3	9.3	9.0	8.4	7.8	7.2	5.5
E^b		5.9	6.6	7.7	13.4	15.3	27.3
E^b per interstitial		3.0	3.3	3.9	4.5	5.1	6.8

in a defect-free cluster of the same size. This defect level has a_1 symmetry and is spread over the central interstitial atoms and the two unique atoms along [001] shaded gray in Fig. 15. This form for I_4 has also been suggested for Si.⁴⁹ This too has gap levels above the valence band top, and recent calculations have presented evidence for this aggregate being present in the positive charge state in the form of the Si:B3 EPR center.⁵⁰ The calculated local modes are listed in Table IV.

VII. ENERGETICS OF THE INTERSTITIAL AGGREGATES

Many of the self-interstitial defects discussed in this article possess the common feature of [001] orientation. In contrast with silicon, the diamond system shows a preference for threefold coordinated self-interstitial defects. In each case where full fourfold coordination is not achieved the defects I_1 - I_3 possess two singly occupied p orbitals, which interact to varying degrees. This phenomenon leads to a number of observable trends.

Energetically there is a clear picture. The formation energy for an aggregate I_n is defined as

$$E_n^f = E_n^d - NE_C,$$

where E_C is the energy per carbon atom of the perfect crystal, and E_n^d is the total energy of the unit cell with N atoms containing the defect. The formation and binding energies of the defects are listed in Table V. Comparing the formation energies (E_n^f) of each I_n aggregate with that of n isolated $I_1^{(001)}$ centers, we find that about 2-3.5 eV is gained through the saving of each dangling bond. We have also listed a ‘‘binding energy’’ defined as the difference in the formation energy of an aggregate of n interstitials and $n \times E^f(I_1)$. As the aggregates get larger the binding energy per interstitial increases.

VIII. PLATELETS

The structure of I_4 suggests a link with the platelet. There have been many models proposed for the platelet extending over more than 40 years,^{9,7,51} but the most recent favor a condensation of carbon interstitials onto a {001} plane.⁹ As all bonds are saturated, an array of I_4 units, as suggested by Humble⁷ and shown schematically in Fig. 17(a), is expected to have particularly low energy. This model is characterized

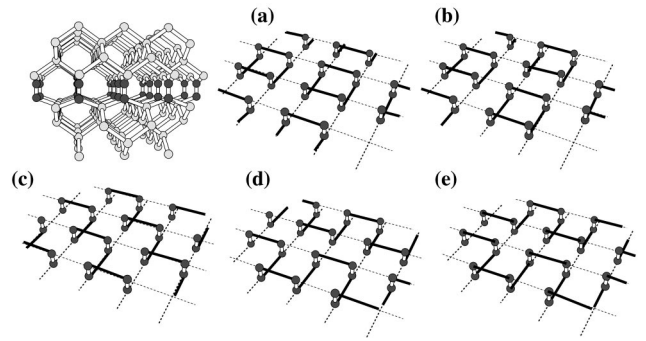


FIG. 17. The proposed structures for the platelet. The large cluster of atoms shows schematically the double layer of atoms made up from the interstitials (shaded sites). (a)–(e) show only these shaded atoms, indicating by the dark lines in each case the type of reconstructions considered. Models (a) and (b) correspond to the dark bonds in Fig. 15. (a) is a regular array of tetrainterstitials and (b) where they are staggered. (c)–(e) consist of the [100] chain and the in- and antiphase [110] chains.

by a C_2 axis running through the diagonals of the squares. A direct consequence of this symmetry is that the [110] and $[\bar{1}\bar{1}0]$ directions are equivalent. The staggered arrangement shown in Fig. 17(b) does not possess a C_2 axis and thus these directions are inequivalent.

It is possible to switch the bond reconstruction from one I_4 unit to a neighboring one with the requirement that each reconstructed bond lies perpendicular to its neighboring reconstructed bonds. Thus one of the reconstructed bonds in Fig. 15 is broken and the atoms with dangling bonds form bonds with neighboring I_4 units. This leads to a plethora of possible models. One such model is shown in Fig. 17(c). Again a C_2 [100] axis runs along [010] and thus the [110] and $[\bar{1}\bar{1}0]$ directions are equivalent.

Now recent transmission electron microscopy studies^{8,9} demonstrate that these directions are not equivalent, restricting which models are consistent with experiment. Figures 17(b), 17(d), and 17(e) show staggered tetrainterstitials and reconstructed chains along $[\bar{1}\bar{1}0]$, all of which are asymmetric between these projections. These are then possible models. It has been suggested that a combination of different topologies might occur.⁹

The TEM studies⁵² have shown that the platelet leads to a displacement of {001} planes by $0.4a_0$ although displacements as low as $0.33a_0$ have been reported for smaller platelets.⁵³ For I_4 , we find that the displacement between the atoms shaded gray in Fig. 15 is $0.34a_0$, in agreement with the latter value. In addition, the calculated infrared-active vibrational modes of I_4 at 1349, 1362, 1401, 1420, 1421, and 1569 cm^{-1} are in reasonable agreement with bands at 1372, 1426, and possibly 1520 and 1540 cm^{-1} , assigned to platelets.⁵⁴ Thus we conclude that platelets formed from aggregates of I_4 are consistent with TEM and infrared absorption measurements.

The models for the platelets were simulated in a periodic system of unit cells consisting of 16 (001) layers of atoms, with four, eight, or 16 atoms per plane depending on the periodicity of the platelet model. The calculations have been performed using the Monkhorst-Pack³⁰ scheme of k points

TABLE VI. Formation energies per interstitial (eV) for the various platelet models (Fig. 17) for the bulk lattice constant and for the relaxed unit cell. For each model the dilation of the lattice in units of a_0 is also reported.

	Model				
	(a)	(b)	(c)	(d)	(e)
Bulk lattice constant	3.58	3.69	4.01	3.82	3.75
Relaxed unit cell	1.04	0.90	1.27	1.20	1.14
Lattice dilation	0.44	0.39	0.38	0.41	0.42

with a 2^3 mesh of points. Formation energies per interstitial, E^f , can be calculated using the formula $E^f = (E_{\text{platelet}} - nE_C)/N$, where E_{platelet} is the total energy of the platelet supercell containing n atoms and N interstitials, and E_C is the energy per atom of pure diamond. The formation energies per interstitial for each of the various models are listed in Table VI. There is a large strain inherent to adding a layer of atoms to a unit cell. Therefore we have also calculated the formation energies for unit cells where the volume of the unit cell is allowed to change. Naturally the formation energies are smaller for the volume relaxed structures, and specifically the minimum is found for the alternating Humble I_4 structure [Fig. 17(b)]. This *does* reflect the asymmetry of the $\langle 110 \rangle$ and $\langle 1\bar{1}0 \rangle$ directions observed experimentally. Furthermore, all the reconstructions investigated give rise to a dilation close to $0.4a_0$. Since the energy differences are small and we have neglected the nucleation processes and strain at the platelet boundaries, one must take care in interpreting these energies. Calculations of the local modes of the periodic systems indicated that bands are present above but close to the Raman refrequency.

The optical transitions associated with platelets cannot be accounted for by these fully reconstructed models, since there are no deep levels associated with these structures. It seems likely that the observed optical activity arises due to disorder in these interstitial aggregate structures, or due to nitrogen, which is always present in relatively large concentrations.

IX. CONCLUSIONS

The *ab initio* theory demonstrates that the small spin-spin dipole tensors in $I_1^{(001)}$ and I_2^{NN} arise from a distributed spin density and the point dipole approximation seriously overestimates the tensors by almost an order of magnitude. The calculations of the tensor reported here have removed this important flaw in the assignments of the $R2$ and $R1$ EPR centers to $[001]$ split-interstitial models for $I_1^{(001)}$ and I_2^{NN} . The calculated piezospectroscopic B tensor for $I_1^{(001)}$ is also

found to be in excellent agreement with the experimental value found for $R2$.

We have analyzed the optical transitions for $I_1^{(001)}$ based on tunneling between two distorted D_2 structures. This is similar to inversion doubling in the ammonia molecule and distinct from a Jahn-Teller system. A Jahn-Teller system requires an orbitally degenerate many-body state. In the case of the single interstitial (D_{2d} symmetry), as explained above, all multiplets are orbitally nondegenerate, and strictly this is not a Jahn-Teller (J-T) system. The potential energy lowering in the calculation due to the lowering of symmetry and splitting of the one-electron doublet has parallels to the J-T problem. The inversion-doubling model leads to the 6 meV splitting of the ground state and provides the mechanism for generating a dipole-allowed transition from the excited state and a forbidden transition from the ground that is made optically active by coupling with a B_1 local mode. This is a different model of the optical properties of I_1 from that of Davies *et al.*⁴³

We also assign the positive charge state of the next-nearest-neighbor model of the di-interstitial to the $3H$ optical center. The symmetry of the defect, its vibrational modes, and the splitting in mixed isotopic material are all consistent with experiment.

The excellent agreement between the calculated D tensor for $I_3^{2\text{NN}}$ and the measured one for the $O3$ EPR center implies that the defects are the same. This assignment suggests a model for I_4 . This fully bonded interstitial defect is expected to be particularly stable and extended defects are made from aggregates of I_4 . This is particularly valuable as it has given us a glimpse of the pathway leading to aggregation of point defects into extended ones.

Several models of the platelet have been investigated, and the lowest-energy one consisting of a staggered array of I_4 defects is consistent with TEM studies showing asymmetry between the $[110]$ and $[\bar{1}0]$ directions, and a $[001]$ displacement between $0.3a_0$ and $0.4a_0$. The calculations also locate vibrational modes of I_4 that are in agreement with infrared data on the platelet.

An important finding is that there are forms of I_2 and I_3 that are more stable than the observed $S=1$ forms of these defects. These may be present in the material but in a diamagnetic form so that experiment has thus far failed to observe them. It follows that introduction rates of radiation defects in diamond are in serious error if only magnetic resonance data are to be relied upon.

ACKNOWLEDGMENTS

S.Ö. thanks NFR and TFR for financial support and computing resources.

¹M. Kohyama and S. Takeda, Phys. Rev. B **46**, 12 305 (1992).

²J. Kim, F. Kirchhoff, W. G. Aulbur, J. W. Wilkins, F. S. Khan, and C. Kresse, Phys. Rev. Lett. **83**, 1990 (1999).

³B. J. Coomer, J. P. Goss, R. Jones, S. Oberg, and P. R. Briddon, Physica B **274**, 505 (1999).

⁴M. Gharaibeh, S. K. Estreicher, and P. A. Fedders, Physica B

- 274, 532 (1999).
- ⁵F. C. Frank, Proc. R. Soc. London, Ser. A **237**, 168 (1956).
- ⁶T. Evans and C. Phaal, Proc. R. Soc. London, Ser. A **270**, 538 (1962).
- ⁷P. Humble, Proc. R. Soc. London, Ser. A **381**, 65 (1982).
- ⁸J. C. Barry, Philos. Mag. A **64**, 111 (1991).
- ⁹P. J. Fallon and L. M. Brown, Philos. Mag. A **72**, 21 (1995).
- ¹⁰D. J. Twitchen, M. E. Newton, J. M. Baker, O. D. Tucker, T. R. Anthony, and W. F. Banholzer, Phys. Rev. B **54**, 6988 (1996).
- ¹¹D. C. Hunt, D. J. Twitchen, M. E. Newton, J. M. Baker, T. R. Anthony, W. F. Banholzer, and S. S. Vagarali, Phys. Rev. B **61**, 3863 (2000).
- ¹²D. Hunt (private communication).
- ¹³S. J. Breuer and P. R. Briddon, Phys. Rev. B **51**, 6984 (1995).
- ¹⁴L. H. Li and J. E. Lowther, J. Phys. Chem. Solids **58**, 1607 (1997).
- ¹⁵R. Jones, P. R. Briddon, and S. Öberg, Philos. Mag. Lett. **66**, 67 (1992).
- ¹⁶J. P. Goss, R. Jones, S. J. Breuer, P. R. Briddon, and S. Öberg, Phys. Rev. Lett. **77**, 3041 (1996).
- ¹⁷R. Jones, J. E. Lowther, and J. Goss, Appl. Phys. Lett. **69**, 2489 (1996).
- ¹⁸J. Walker, J. Phys. C **10**, 3867 (1977).
- ¹⁹L. Allers, A. T. Collins, and J. Hiscock, Diamond Relat. Mater. **7**, 228 (1998).
- ²⁰J. W. Steeds, T. J. Davis, S. J. Charles, J. M. Hayes, and J. E. Butler, Diamond Relat. Mater. **8**, 1847 (1999).
- ²¹K. Iakubovskii, Ph.D. thesis, Katholieke Universiteit Leuven, 2000.
- ²²D. Twitchen, M. E. Newton, and J. M. Baker (private communication).
- ²³A. Mainwood, F. P. Larkins, and A. M. Stoneham, Solid-State Electron. **21**, 1431 (1978).
- ²⁴T. Evans and Z. Qi, Proc. R. Soc. London, Ser. A **381**, 159 (1982).
- ²⁵G. S. Woods, Proc. R. Soc. London, Ser. A **407**, 219 (1986).
- ²⁶P. R. Briddon, R. Jones, and M. I. Heggie, in *Proceedings of the International Conference on New Diamond Science and Technology*, edited by R. Messier, J. T. Glass, J. E. Butler, and R. Roy (Materials Research Society, Pittsburgh, 1991), p. 63.
- ²⁷P. R. Briddon, R. Jones, and M. I. Heggie, Mater. Sci. Forum **83-87**, 457 (1991).
- ²⁸R. Jones and P. R. Briddon, in *Identification of Defects in Semiconductors*, Vol. 51A of *Semiconductors and Semimetals*, edited by M. Stavola (Academic Press, Boston, 1998), Chap. 6.
- ²⁹J. Coutinho, R. Jones, S. Öberg, and P. R. Briddon, Phys. Rev. B **62**, 10 824 (2000).
- ³⁰H. J. Monkhorst and J. D. Pack, Phys. Rev. B **13**, 5188 (1976).
- ³¹A. Resende, R. Jones, S. Öberg, and P. R. Briddon, Phys. Rev. Lett. **82**, 2111 (1999).
- ³²J. C. Slater, *Quantum Theory of Atomic Structure* (McGraw Hill, New York, 1960), Vol. 2.
- ³³K. L. Brower, Phys. Rev. B **4**, 1968 (1971).
- ³⁴The localization length $1/\kappa$ for an orbital ϕ is defined as the asymptotic behavior of the orbital, $\phi \sim e^{-\kappa r}$, which depends on the specific defect.
- ³⁵G. D. Watkins, in *Early Stages of Oxygen Precipitation in Si*, edited by R. Jones, Vol. 1 of NATO Advanced Study Institute, Series 3: High Technology (Kluwer Academic Publishers, Dordrecht, 1996), p. 1.
- ³⁶D. Liberman, Phys. Rev. B **62**, 6851 (2000).
- ³⁷R. Jones, J. Phys. C **21**, 5735 (1988).
- ³⁸U. von Barth and L. Hedin, J. Phys. C **5**, 1629 (1972).
- ³⁹D. W. Palmer, Ph.D. thesis, University of Reading, 1961.
- ⁴⁰L. Allers and A. Mainwood, Diamond Relat. Mater. **7**, 261 (1998).
- ⁴¹M. E. Newton, in *Properties and Growth of Diamond*, edited by G. Davies (INSPEC, Institute of Electrical Engineers, London, 1994), Chap. 5.2.
- ⁴²E. A. Faulkner and J. N. Lomer, Philos. Mag. B **7**, 1995 (1962).
- ⁴³G. Davies, H. Smith, and H. Kanda, Phys. Rev. B **62**, 1528 (2000).
- ⁴⁴D. J. Twitchen, M. E. Newton, J. M. Baker, W. F. Banholzer, and T. Anthony, Diamond Relat. Mater. **8**, 1101 (1999).
- ⁴⁵D. J. Twitchen, D. C. Hunt, M. E. Newton, J. M. Baker, T. R. Anthony, and W. F. Banholzer, Physica B **274**, 628 (1999).
- ⁴⁶J. W. Steeds, S. Charles, T. J. Davis, A. Gilmore, J. Hayes, D. Pickard, and J. E. Butler, Diamond Relat. Mater. **8**, 91 (1999).
- ⁴⁷The convention chosen here is that the B_1 irreducible representation has odd parity under reflection in the plane containing the two interstitials.
- ⁴⁸H. Sternschulte, K. Thonke, R. Sauer, and S. Koizumi, Phys. Rev. B **59**, 12 924 (1999).
- ⁴⁹N. Arai, S. Takeda, and M. Kohyama, Phys. Rev. Lett. **78**, 4265 (1997).
- ⁵⁰B. J. Coomer, J. P. Goss, R. Jones, S. Öberg, and P. R. Briddon, J. Phys.: Condens. Matter **13**, L1 (2000).
- ⁵¹A. R. Lang, Proc. Phys. Soc. London **84**, 871 (1964).
- ⁵²D. Cherns, K. Kaneko, A. Hovsepian, and A. Lang, Philos. Mag. A **75**, 1553 (1997).
- ⁵³J. C. Barry, L. A. Bursill, and J. L. Hutchison, Philos. Mag. A **51**, 15 (1985).
- ⁵⁴G. S. Woods, Philos. Mag. Lett. **59**, 339 (1989).